Characterization of a radiation-pressure-driven micromechanical oscillator

Mani Hossein-Zadeh,[1] Hossein Rokhsari,[1] Ali Hajimiri,[2] and Kerry J. Vahala[1]
[1]*Department of Applied Physics, California Institute of Technology, Pasadena, California 91125, USA*
[2]*Department of Electrical Engineering, California Institute of Technology, Pasadena, California 91125, USA*
(Received 16 February 2006; published 18 August 2006)

We present for the first time a detailed experimental study of the oscillation frequency, linewidth, RF spectrum and the phase noise of a radiation-pressure-driven micromechanical oscillator in a microtoroid geometry. Through this study we identify the critical parameters for optimal operation of this device and derive key expressions for tailoring the desired characteristics. The outcome of this study paves the ground for exploiting this unique phenomenon in photonic systems as well as fundamental studies in macroscopic quantum mechanics.

DOI: 10.1103/PhysRevA.74.023813 PACS number(s): 42.65.Sf, 42.60.Da, 05.40.Ca, 07.10.Cm

I. INTRODUCTION

Recently a unique class of oscillators based on strong coupling between high-Q optical and mechanical modes of silica microtoroids has been demonstrated [1–4]. In these optomechanical oscillators a continuous source of pump laser power generates mechanical vibrations at radio frequencies (RF) without utilizing any sort of external feedback system. These oscillations imprint themselves onto the transmitted optical power, now an optical carrier for the RF frequencies. Realization of this effect in ultrahigh-Q microtoroidal optical resonators [5] relies on their unique geometrical and structural properties that support both high-Q optical and mechanical modes and enable energy exchange between them.

This effect can benefit applications in RF micromechanical oscillator-on-a-chip and all-optical frequency reference devices. From a more fundamental point of view the optomechanical interaction introduces a unique platform for exploring quantum optical phenomena such as entanglement, squeezing, and back-action noise [6–9].

In this work we perform a detailed experimental study and characterize the operation of these devices. This is required for the ultimate goal of utilizing these oscillators in photonic systems and quantum optical applications. We explore the role of different adjustable parameters as well as intrinsic features that govern the behavior of this device. Specifically we study the impact of optical frequency detuning and optical input power on the oscillation amplitude, spectral purity, linewidth and phase noise performance of these oscillators. The outcome of our measurements is an essential step towards optimization of all-optical frequency-reference devices based on optomechanical systems, as well as identifying unique aspects of this phenomenon, which may benefit fundamental research.

II. A BRIEF REVIEW OF OPTOMECHANICAL OSCILLATION IN MICROTOROIDS

In a high-Q toroidal microresonator, the radiation pressure of the circulating optical power exerts a radial force on the silica microtoroid that expands the cavity structure and consequently decreases the frequency of the optical resonance (ω_0). If the frequency of the optical pump wave (ω) is originally higher than the cavity resonance ($\Delta\omega=\omega-\omega_0>0$), this resonant frequency shift decreases the circulating optical power, hence the radiation pressure drops and subsequent restoration of the mechanical deformation resumes the process. The response of the mechanical structure to the radiation pressure variations is not instantaneous and it is delayed by the finite speed of the acoustic wave in the mechanical structure. This delay is quantified through the period of the mechanical motion ($\tau_{\mathrm{mech}}=2\pi/\Omega$). When the positive feedback produced by the circulating optical power is large enough to overcome the mechanical loss a periodic motion of the microtoroid cavity at an eigenmechanical frequency of the toroidal structure (Ω) ensues. The periodic motion modulates the circulating optical power and manifests itself as amplitude modulation of the optical output power. This optomechanical oscillation is regenerative, exhibiting classic threshold behavior and requires no external modulation of the pump wave [1]. Note that the bandwidth of the positive feedback mechanism (i.e., the response of the circulating optical power to the detuning) is determined by the cavity build-up time ($\tau_{\mathrm{opt}}=Q_{\mathrm{tot}}/\omega_0=1/2\delta$ where 2δ is the bandwidth of the optical resonance).

Figures 1(a) and 1(b) illustrate the optomechanical oscillation mechanism. Notice that the mechanical and the optical resonators are co-located in the same structure. In other words a mechanical resonator and an optical cavity, embodied within the microtoroid, are parametrically coupled despite a seven order-of-magnitude difference in their resonant frequencies (10^7 Hz as opposed to 10^{14} Hz). Figure 1(c) shows a rendering of the microtoroid undergoing flexural vibrations.

Usually evanescent coupling through a phase-matched waveguide (fiber taper [2]) is used to couple light into and out of the optical resonator. The optical power at the coupling junction (P_j) is the only input power to the system [Fig. 1(a)]. Table I summarizes the notation used for the modal parameters of the mechanical resonator and the optical cavity.

Different quality factors in this system are defined as follows:

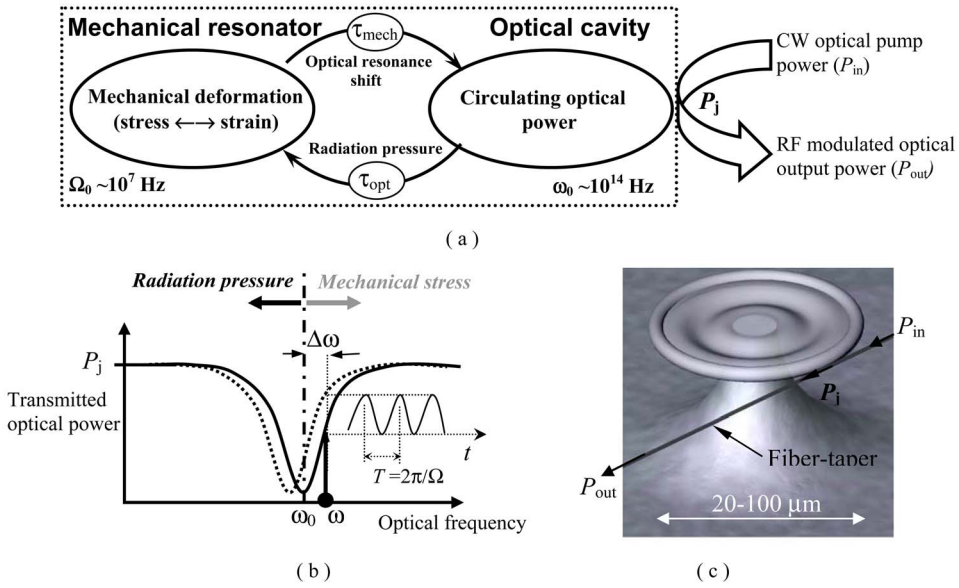

FIG. 1. (Color online) (a) Optomechanical oscillation mechanism. (b) Illustration of the optomechanical oscillation in optical frequency domain. (c) A rendering of the microtoroid undergoing flexural vibrations.

$$Q_{\mathrm{mech}} = \frac{\Omega_0}{\Delta\Omega_0}, \quad Q_0 = \frac{\delta_0}{2\omega_0}, \quad Q_{\mathrm{tot}} = \frac{\omega_0}{2\delta}, \quad Q_{\mathrm{ext}} = \frac{Q_0 Q_{tot}}{Q_0 - Q_{tot}}. \tag{1}$$

Q_0, Q_{tot}, Q_{ext} are the intrinsic, total, and external optical quality factors [10,11] and Q_{mech} is the intrinsic mechanical quality factor.

The theory of the optomechanical oscillation has been explored in different regimes in previous publications [1–3]. As explained in Ref. [2], the simplest model for the optomechanical oscillation can be expressed by two coupled differential equations that govern the dynamics of the optical field and the mechanical motion

$$\ddot{r}(t) + \gamma_0 \dot{r}(t) + \Omega^2 r(t) = F_{rp} = \frac{2\pi n}{c m_{\mathrm{eff}}} \frac{c n \varepsilon_0}{2} s |E(t)|^2, \tag{2}$$

$$\dot{E}(t) + E(t)\left[\frac{\omega}{2Q_{\mathrm{tot}}} - i\Delta\omega + i\frac{\omega_0}{R_0} r(t)\right] = i\sqrt{\frac{(2/cn\varepsilon_0 s')P_j \omega}{\tau_0 Q_{\mathrm{ext}}}}, \tag{3}$$

where $r(t)$ is the radial displacement of the microtoroid $[r(t)=r_{\max}\cos(\Omega t)]$, $E(t)$ is the electrical field of the circulating optical wave, n is the effective refractive index of the optical mode, c is the speed of light, and $\tau_0(=2\pi R_0 n/c)$ is the photon roundtrip time in the optical resonator. s and s' are the cross sectional areas of the optical modes in the cavity and the waveguide, respectively. γ_0 is the loss rate due to mechanical dissipation (we have assumed that the mechanical motion is subject to a frictional force with the frictional constant $m_{\mathrm{eff}}\gamma_0$). m_{eff} is the effective resonator mass for radial motion and is defined based on the total energy (U) stored in the mechanical mode such that $m_{\mathrm{eff}} = 2U/(r^2_{\max}\Omega^2)$ where $r_{\max}$ is the amplitude of the mechanical vibration in the radial direction. F_{rp} is the radiation force associated with the circulating optical power. Note that m_{eff} is different for each mechanical eigenmode and can be estimated by finite element modeling of the corresponding mechanical mode.

TABLE I. Modal parameters of the optical cavity and the mechanical resonator. Note that the optical mode is excited by the waveguide (fiber-taper) while the mechanical mode is excited by the radiation pressure of the circulating optical power.

Modal property	Intrinsic	Excited
Mechanical resonant frequency	Ω_0	Ω
Mechanical oscillation linewidth	$\Delta\Omega_0$ $(=\gamma_0)$	$\Delta\Omega$
Frequency of the optical mode	ω_0	$\approx\omega_0$
Linewidth of the optical mode	$2\delta_0$	2δ

At a given temperature and ambient pressure, the oscillation frequency (Ω_0) and linewidth $(\Delta\Omega_0)$ of each mechanical eigenmode in the passive resonator are determined by the geometry of the silica microtoroid and silicon pillar as well as their structural properties (i.e., Young modulus, internal dissipation, etc.). Based on experimental results, within the accuracy of our measurements and the temperature gradients involved in our system, thermal effects mainly affect Ω_0 but not $\Delta\Omega_0$. However at very low temperatures due to the fundamental changes in the loss mechanisms, thermal effects can significantly modify Q_{mech} and $\Delta\Omega_0$ [12]. Also, ambient pressure translates to an effective frictional force for the mechanical motion and therefore it affects both Ω_0 and $\Delta\Omega_0$ [13]. Since all of our measurements are performed in atmospheric pressure, we have not considered the ambient pressure as a variable in the equations.

Before initiation of the regenerative oscillations (below threshold regime), the presence of the circulating optical power in the resonator effectively modifies the mechanical loss (γ_0) and the resonant frequency (Ω_0) of the mechanical resonator such that [1]

$$\ddot{r}(t) + \gamma \dot{r}(t) + \Omega^2 r(t) = 0, \tag{4a}$$

$$\gamma = \gamma_0\left(1 - \frac{P_{\mathrm{j}}}{P_{\mathrm{th}}(\Delta\omega)}\right), \tag{4b}$$

$$\Omega = \Omega_0[1 + \eta_P(\Delta\omega)P_{\mathrm{j}}]. \tag{4c}$$

$P_{\mathrm{th}}(\Delta\omega)$ can be interpreted as the threshold optical pump power for initiation of self-sustained mechanical oscillation where the optomechanical gain overcomes the mechanical loss. When $(P > P_{\mathrm{th}})$ there is a net power transfer from the optical pump to the mechanical oscillation. Below threshold $(P < P_{\mathrm{th}})$ the oscillator is thermally driven and the presence of the circulating optical power only reduces the mechanical loss factor [Eq. (4b)]. $\Omega_0\eta_P(\Delta\omega)P_j$ is the mechanical resonant frequency shift due to the presence of circulating optical power in the microtoroid. η_p essentially combines the thermal drift due to optical absorption in the structure and the optical spring effect [14] due to radiation pressure. $P_{\mathrm{th}}(\Delta\omega)$ and $\eta_P(\Delta\omega)$ are determined by optical coupling and physical parameters of the microresonator. Note that since the loss induced oscillation frequency shift $(\sqrt{\Omega_0^2 - \gamma^2/4})$ is negligible, γ does not appear in Eq. (4c) (see Appendix A).

For small mechanical frequencies $(\Omega \ll 2\delta)$ using Eqs. (2)–(4), an approximate closed form expression for $P_{\mathrm{th}}(\Delta\omega)$ has been derived in Ref. [1] Employing a different approach based on slowly varying envelope approximation and coupled mode analysis a general expression for $P_{\mathrm{th}}(\Delta\omega)$ can be derived that is valid for even large mechanical frequencies (arbitrary Ω) [3]

$$P_{\mathrm{th}}(\Delta\omega) = \left(\frac{2\Omega_0^2\omega_0^2 m_{\mathrm{eff}}R_0^2}{Q_{\mathrm{mech}}Q_0Q_{\mathrm{tot}}}\right)H(\Delta\omega), \tag{5}$$

$$H(\Delta\omega) = \frac{|1 + K + 2i\Delta\omega Q_0\omega_0^{-1}|^2}{4K} \times\left(\frac{1}{1 + 4Q_{\mathrm{tot}}^2\omega_0^{-2}\Delta\omega_{AS}^2} - \frac{1}{1 + 4Q_{\mathrm{tot}}^2\omega_0^{-2}\Delta\omega_S^2}\right)^{-1}, \tag{6}$$

where $\Delta\omega_{\mathrm{AS}} = \Delta\omega + \Omega$ and $\Delta\omega_S = \Delta\omega - \Omega$ are the frequency offsets of the anti-Stokes and Stokes modes in the optical cavity. K $(=Q_0/Q_{\mathrm{ext}})$ is the normalized optical coupling coefficient (K is optimized and kept constant during each measurement). Deriving a general expression for η_P is more complicated since it involves the thermodynamical behavior of the system as well as radiation pressure. However a semiempirical expression can be derived that explains the overall behavior of η_P as a function of $\Delta\omega$

$$\eta_P = A\left(\frac{1}{\Delta\omega^2 + \delta^2}\right) + B\left[\frac{\Delta\omega}{(\Delta\omega^2 + \delta^2)^2}\right], \tag{7}$$

where A and B are the proportionality factors for the optical spring effect and the optical absorption effect, respectively. Derivation of the above expression is presented in Appendix A. Temporal behavior and the threshold optical power of the optomechanical oscillation have been shown to be in good agreement with theoretical predictions [3,4]. The behavior of mechanical oscillation frequency and linewidth, however, have not been addressed yet.

Below threshold $(P_{\mathrm{th}} > P_{\mathrm{j}})$ the presence of optical power modifies the oscillation frequency (Ω) through optical absorption and the optical spring effect, and the linewidth is equal to mechanical loss $(\Delta\Omega = \gamma)$. In this regime, Eqs. (4b) and (4c) can explain the behavior of the oscillation frequency and linewidth. Above threshold (where the gain overcomes the mechanical loss) Eq. (4c) can still explain the behavior of the oscillation frequency, but the oscillation linewidth is no longer described by Eq. (4b). In the above-threshold regime oscillation linewidth is limited by the presence of different noise mechanisms in the oscillator system. A detailed theoretical study of the oscillation linewidth in this regime requires a modified system of equations that includes the noise in the optical pump power as well as thermal noise in the microresonator structure and is beyond the scope of this paper. However, the above threshold linewidth may be explained using the general theory of line narrowing in self-sustained oscillators, which has been developed in the context of optical oscillators (Schawlow-Townes line narrowing in lasers) as well as electronic oscillators [15–17]. This is because all oscillators that are fundamentally limited by a white noise source (spontaneous emission in lasers and Johnson noise in electronic oscillators) are essentially governed by similar differential equations with only differences in the physical interpretation of the coefficients and noise terms. In a thermally limited oscillator this theory states that the oscillation linewidth $(\Delta\Omega)$ is inversely proportional to the oscillator output power (P_d) such that:

$$\Delta\Omega = \frac{k_B T}{2P_d}(\Delta\Omega_0)^2. \tag{8}$$

Through a detailed study of the short-term stability of the optomechanical oscillator we have demonstrated that in the above-threshold regime the measured mechanical oscillation linewidth is in good agreement with Eq. (8) [18]. In other words, at room temperature the thermomechanical noise, also referred to as Brownian motion, is the dominant noise mechanism in the microtoroid optomechanical oscillator. It is useful to rewrite Eq. (8) in terms of measurable parameters

$$\Delta\Omega = \left(\frac{4k_B T Q_{\mathrm{tot}}^2}{m_{\mathrm{eff}}\Omega_0^2 R_0^2}\right)\frac{\Gamma_\Omega^2\Delta\Omega_0}{M^2}, \tag{9}$$

where M is the optical modulation depth (induced by resonator motion) and Γ_Ω is the optical modulation transfer function [19] [derivation of Eq. (9) can be found in Appendix B]. Equation (9) is a very useful expression for comparison between experimental data and theoretical prediction and will be used in Sec. III C.

A careful look at the dynamical equations governing the oscillator behavior shows oscillation amplitude, frequency spectrum and linewidth of the optomechanical oscillator are all controlled by two principal external parameters: optical input power (P_j) and optical frequency detuning $(\Delta\omega)$. In order to show the typical behavior of the threshold optical power and oscillation linewidth for above and below threshold regimes we have calculated these quantities for a typical

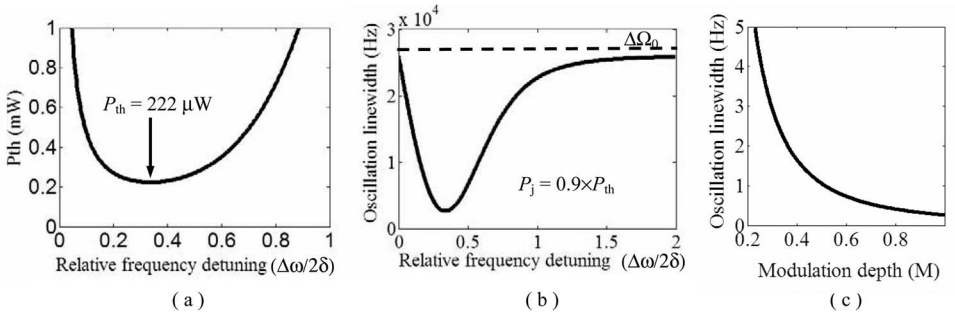

FIG. 2. (a) Calculated threshold optical power versus relative optical frequency detuning. (b) Oscillation linewidth below threshold versus relative optical frequency detuning. (c) Oscillation linewidth above threshold versus optical modulation depth (M). All calculations are for a optomechanical oscillator with $R_0=30$ μm, $Q_{tot}=1.5\times10^6$, $Q_0=5.5\times10^6$, $Q_{mech}=2\times10^3$, $m_{eff}=2.3\times10^{-11}$ kg (these values are chosen based on the experimental and simulated values for the fourth mechanical eigenmode of the device under test).

optomechanical oscillator with $R=30$ μm, $Q_{tot}=1.5\times10^6$, $Q_0=5.5\times10^6$, $Q_{mech}=2\times10^3$, $m_{eff}=2.3\times10^{-11}$ kg (these values are chosen according to the experimental and simulated values for the fourth mechanical eigenmode of the device under test in this work). Figure 2(a) shows the threshold optical power for optomechanical oscillation versus relative optical frequency detuning from resonance ($\Delta\omega/2\delta$). The minimum threshold optical power occurs at $\Delta\omega/2\delta\approx0.35$. Throughout this paper the threshold power for each optical mode corresponds to this minimum value and is indicated by P_{th}. Figure 2(b) shows below threshold oscillation linewidth ($\Delta\Omega=\gamma$) versus $\Delta\omega/2\delta$. Note that in this regime the oscillator is thermally driven and the optomechanical interaction only modifies the effective mechanical dissipation (γ). Oscillation linewidth is calculated using Eq. (4b) where $P_{th}(\Delta\omega)$ is substituted from Eq. (5). Oscillation linewidth possesses a minimum at the same detuning for which $P_{th}(\Delta\omega)$ is minimized (maximum optomechanical gain). As expected at large detuning $\Delta\omega>4\delta$ (small optomechanical gain) $\Delta\Omega$ approaches the asymptotic value of $\Delta\Omega_0$. Figure 2(c) shows the oscillation linewidth above threshold versus optical modulation depth [Eq. (8)]. Notice that for $M>0.5$ (large oscillation amplitude) the oscillation linewidth enters the sub-Hertz regime.

III. EXPERIMENTAL SETUP

Figure 3(a) is a side-view SEM picture of the microtoroidal resonator. The silica microtoroid has a principal diameter of 60 μm. The silicon pillar diameter at the silica-silicon junction is 5 μm. The small size of the silicon pillar at the junction reduces the mechanical loss to the pillar and it is critical for achieving low oscillation threshold powers especially for higher order mechanical modes. To make this structure, we have added an extra step to the conventional microtoroid fabrication process [5] by performing a second XeF_2 etch after CO_2 reflow process. During this second dry etch the diameter of the silicon pillar is reduced further to tune the contact diameter to the desired value. Standard fiber-taper coupling was used to couple optical power to the

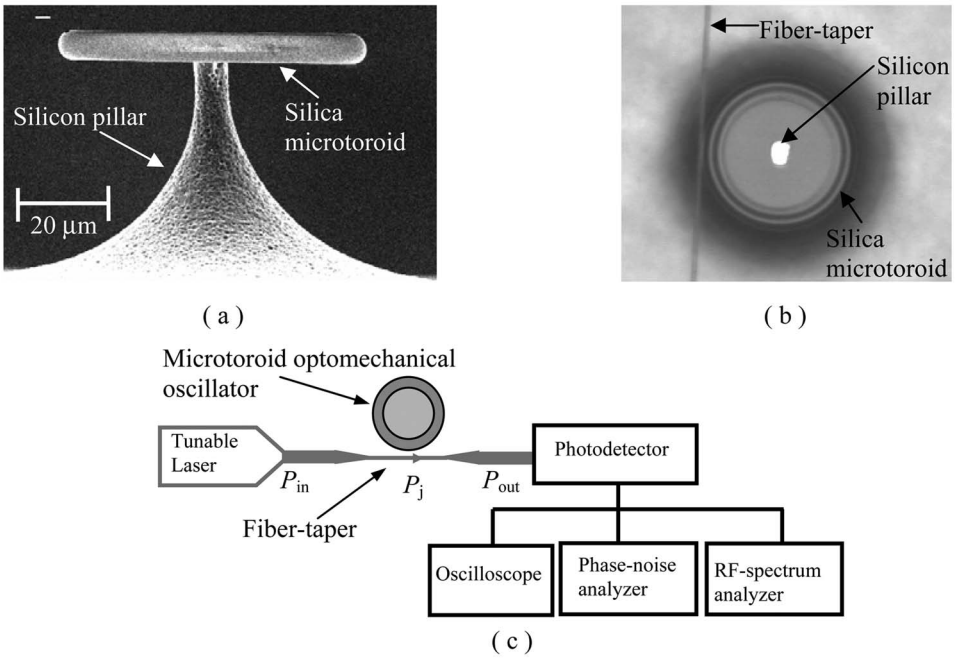

FIG. 3. (a) Side-view scanning-electron micrograph (SEM) of the microtoroid used in this study. (b) Top view photomicrograph of the microtoroid optomechanical oscillator coupled to a fiber taper. (c) Schematic diagram of the experimental arrangement.

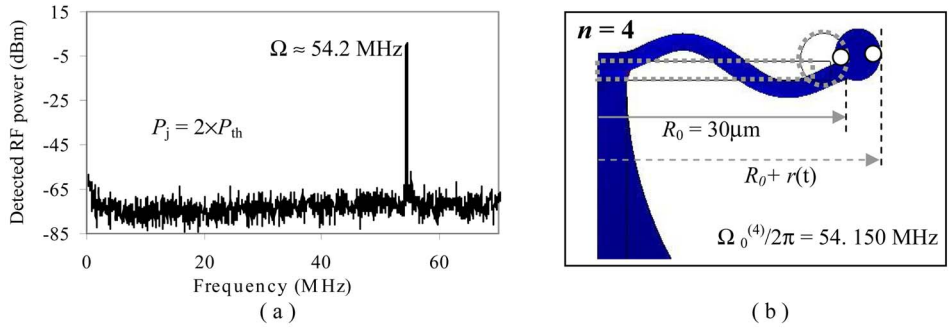

FIG. 4. (Color online) (a) RF spectrum of the photodetector output while the fourth mechanical mode is excited. (b) Finite element modeling of the fourth flexural mechanical eigenmode. The deformation (solid black) is exaggerated to show the deviation from equilibrium (dotted line). The small white circles indicate the cross section of the optical mode.

microtoroid and the coupling gap was controlled by a nanopositioner [20]. Figure 3(b) shows the top-view photomicrograph of the microtoroid coupled to the fiber taper. The optical power at the coupling junction (P_j) is calculated by substituting the measured off resonance values of the optical input power (P_{in}) and optical output power (P_{out}) into the expression $P_j=(P_{out}P_{in})^{1/2}$ (to account for the taper-fiber loss). The optical modes of this microtoroid had intrinsic quality factors between 4×10^6 and 7×10^6. Figure 3(c) shows a schematic diagram of the experimental arrangement. A tunable laser provides CW optical power around $\lambda = 1550$ nm with a linewidth of 300 kHz. The optical pump power stimulates the optomechanical oscillation that results in amplitude modulation of the transmitted optical power. Notice that the laser input power serves both as the pump and the probe for the optomechanical oscillation. A photodetector with a bandwidth of 120 MHz was used to convert the optical amplitude modulation into a photocurrent signal.

The detected signal is analyzed using an RF spectrum analyzer. A delay discriminator based phase noise analyzer is used to measure the phase noise performance of the optomechanical oscillator and extract the oscillation linewidth in the sub-Hertz regime. The optical mode spectrum and the optical frequency detuning are measured with an oscilloscope.

The first four mechanical modes of this microtoroid had resonant frequencies of 2.4 MHz, 15.92 MHz, 39.64 MHz, and 54. MHz, respectively. Due to its low threshold power the fourth flexural mechanical mode with a measured mechanical quality factor (Q_{mech}) of about 2100 has been chosen for this study. For an optical mode with $Q_0=5.5\times10^6$ and optimized optical coupling ($K\sim2.5$) the measured optical threshold power (P_{th}) was about 250 μW (which is in agreement with theoretical prediction in Fig. 2(a) that is calculated based on the same values for the resonator parameters).

Figure 4(a) shows the RF spectrum of the detected optical power when the fourth mechanical eigenmode is excited (threshold power 250 μW). The clean spectrum indicates that at the chosen optical coupling regime, P_{th} for other mechanical modes was well above 250 μW.

Figure 4(b) shows the finite element modeling of the microtoroid deformation when the fourth flexural mechanical mode is excited. The deformation (solid shape) is exaggerated to show the deviation from equilibrium (dashed line). The calculated eigen-frequency is in good agreement with the measured frequency (54.2 MHz). The estimated value of the effective resonator mass (m_{eff}) for this mode is 2.3×10^{-11} kg. As evident from Fig. 4(b) the mechanical displacement of this mode moves the optical mode volume mainly in the radial direction.

IV. EXPERIMENTAL RESULTS

A. Oscillation amplitude and linearity

Figure 5(a) shows the transmitted optical power at $P_j=1.5\times P_{th}$ ($P_{th}=250$ μW) as the optical frequency of the pump wave is slowly swept (10 sweep/sec) through the toroid resonant frequency. The triangular shape of the transmission (as opposed to a Lorentzian) is an artifact of the thermo-optical resonance shift [21] in conjunction with the slow scan rate. For higher scan rates that are faster than the toroid thermal response or for lower pump powers, the

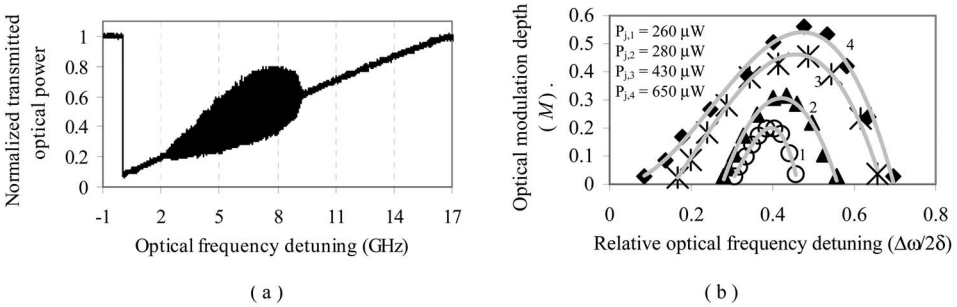

FIG. 5. (a) Transmitted optical power measured as pump frequency is slowly scanned through the optical resonant frequency ($P_j=1.5\times P_{th}=375$ μW). (b) Optical modulation depth (M) against relative optical frequency detuning at different optical input powers.

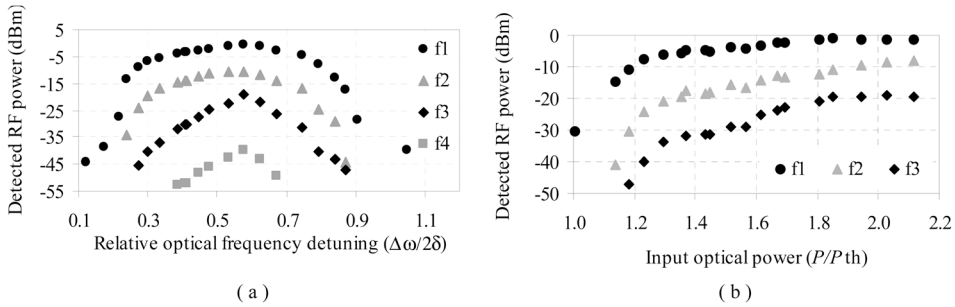

FIG. 6. (Color online) (a) Measured RF power at the fundamental oscillation frequency (f_1=54.2 MHz) and its second (f_2=108.4 MHz), third (f_3=162.6 MHz), and fourth (f_4=216.8 MHz) harmonics plotted against relative optical frequency detuning from resonance (optical input power was $2\times P_{\text{th}}$=500 μW). (b) Measured RF power at fundamental oscillation frequency (f_1) and its second (f_2) and third harmonics (f_3) plotted against relative optical input power. $\Delta\omega$ is kept at its optimum value during the measurement.

underlying Lorentzian spectral profile (and hence the Q_0) are readily observed. The measured values of Q_{tot} and Q_0 were 1.5×10^6 and 5.5×10^6, respectively. According to the above analysis, at a certain optical frequency detuning ($\Delta\omega$) the optomechanical gain overcomes the mechanical loss and the ensuing regenerative oscillation of the microtoroid radius modulates the amplitude of the transmitted optical power. This modulation appears as the dark, broadened region in the pump scan of Fig. 5(a). Because the pump wavelength is scanned at a slow rate of 10 scan/sec (each scan spans 170 GHz of the optical spectrum in 0.1 sec), the MHz-rate mechanical oscillation is not resolved in this figure and appears instead as a broadening in the transmitted optical power. As expected, the oscillation occurs when the pump frequency is blueshifted with respect to cavity mode where the optomechanical gain is positive [1]. We note that redshifted pumping of the optical mode is expected to induce damping of the mechanical motion, however this is difficult to observe as this pump to resonant frequency arrangement ($\Delta\omega<0$) is not thermally stable; hence the abrupt vertical line in the triangular-shaped pump transmission scan [Fig. 5(a)] [21].

Figure 5(b) shows the measured optical modulation depth (which, for small depths, is proportional to the mechanical oscillation amplitude) versus the relative frequency detuning from the resonance ($\Delta\omega/2\delta$) at different optical input powers. At each optical input power level there is an optimum detuning that maximizes the modulation depth. Notice that the optimum detuning increases as the optical power grows. The maximum modulation depth occurs when $\Delta\omega/2\delta$ is between 0.4 and 0.5. We note that in these and other data the actual optical frequency detuning is determined by first measuring the loaded optical linewidth 2δ at very low optical input power (where thermal effects are negligible and hence the measured, optical mode profile has a Lorentzian shape). This information can then be used with measurements of transmitted power to ascertain detuning at arbitrary pump levels or scan rates.

Since the optical transfer function of an optical resonator has a Lorentzian shape, modulation of the optical resonance results in nonlinear amplitude modulation of the transmitted optical power. This nonlinear transfer function manifests itself through the appearance of harmonics of the mechanical eigen frequencies within the optical power modulation spectrum. These harmonics are readily observed in the RF spectrum of the detected optical power. We have measured the RF powers of each frequency component up to the fourth harmonic as a function of optical power and optical frequency detuning. Figure 6(a) shows the detected RF power at the fundamental frequency of the fourth mechanical eigenmode and its harmonics plotted against relative optical frequency detuning from resonance (optical input power is $2\times P_{\text{th}}$=500 μW). Figure 6(b) shows the detected RF power at the fundamental frequency of the fourth mechanical eigenmode and its harmonics plotted against relative optical input power to the microtoroid ($\Delta\omega$ is set to its optimal value at each power level). The second and third harmonic suppression ratios are 20 dB and 35 dB at $1.2\times P_{\text{th}}$ and they gradually decrease to 7 dB and 17 dB at $2\times P_{\text{th}}$.

B. Oscillation phase noise

Phase noise is one of the most important characteristics of any self-sustained oscillator. To measure phase noise of the mechanical oscillation we utilize the detected photocurrent, which contains a replica of the mechanical motion (and hence the phase noise of this motion). The replica nature of this component results because it is generated (at the detector) as the product of the pump field with Stokes and

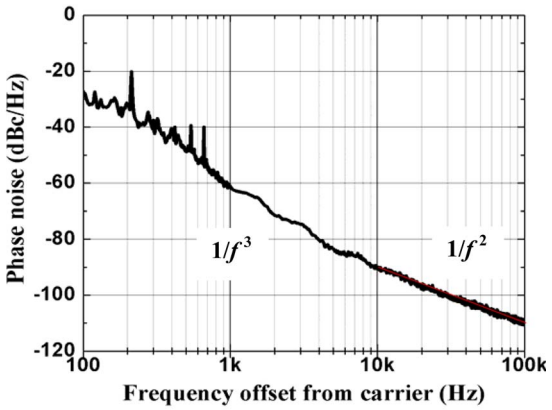

FIG. 7. (Color online) A typical phase noise spectrum of the optomechanical oscillation.

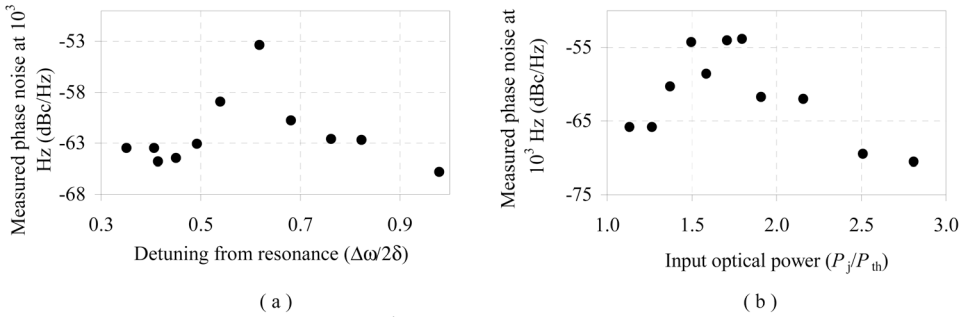

FIG. 8. (Color online) (a) Phase noise of the optomechanical oscillator measured at 10^3 Hz offset from the carrier frequency (54.2 MHz) plotted against relative optical frequency detuning from resonance. Optical input power is about $2\times P_{\text{th}}=500$ μW. (b) Phase noise of the optomechanical oscillator measured at 10^3 Hz offset from the carrier frequency at $\Delta\omega/2\delta\approx 0.5$, plotted against relative optical input power.

anti-Stokes side bands. Figure 7 shows a typical result of measurement of the phase noise spectrum of the fourth mechanical mode using the phase noise analyzer illustrated in Fig. 3. We observe a dependence of $1/f^3$ at offset frequencies (Δf) between 100 Hz and 10 kHz and a dependence of $1/f^2$ at offsets larger than 10 kHz (gray area). The observation of these two regimes is in good agreement with general phase noise behavior of closed-loop oscillators [22–24]. The $1/f^3$ regime is a signature of $1/f$ or "flicker noise" in the system while the appearance of $1/f^2$ regime is mainly due to the presence of the white noise [23].

We have characterized the phase noise performance of the optomechanical oscillator by measuring the phase noise at selected offset frequencies in the $1/f^3$ and $1/f^2$ regions (10^3 Hz and 10^5 Hz, respectively). Figure 8(a) shows the phase noise of the optomechanical oscillator measured at 10^3 Hz offset (Δf) from the carrier frequency (54.2 MHz), plotted against relative optical frequency detuning from the resonance ($\Delta\omega/2\delta$) at 500 μW ($2\times P_{\text{th}}$) optical input power. The phase noise increases by about 10 dB around $\Delta\omega/2\delta \sim 0.6$ in the vicinity of the frequency detuning at which the oscillation amplitude is maximized [Fig. 5(b)].

Figure 8(b) shows the phase noise of the optomechanical oscillator measured at 10^3 Hz offset from the carrier frequency and at $\Delta\omega/2\delta\approx 0.5$ plotted against relative optical input power. The phase noise increases with input power from P_{th} to about 1.7 P_{th} and then gradually decreases as we increase the power further. Due to the complex nature of the $1/f$ noise (which results in $1/f^3$ dependence in the phase noise spectrum), the physical interpretation of these results is not trivial. However it is clear that the mechanisms that are responsible for this process are related to the magnitude of the circulating optical power in the resonator and therefore may be associated with thermal gradients in the resonator structure. Figure 9(a) shows the phase noise of the optomechanical oscillator measured at 10^5 Hz offset from the carrier frequency (54.2 MHz), plotted against relative optical frequency detuning at 500 μW($2\times P_{\text{th}}$) optical input power. At the optimal detuning (maximum oscillation amplitude) high frequency phase noise is minimized. Figure 9(b) shows the phase noise of the optomechanical oscillator measured at 10^5 Hz offset from the carrier frequency and for optical detuning $\Delta\omega/2\delta\approx 0.5$, plotted against relative optical input power. As evident from the figure phase noise decreases with the optical power. Since, in the $1/f^2$ regime, the phase noise spectral density is proportional to the short-term linewidth $\Delta\Omega$ [24], this behavior shows that $\Delta\Omega$ varies inversely with the oscillation amplitude (the precise dependence being inverse quadratic). This short-term linewidth amplitude dependence links the source of phase noise to fundamental noise as described in greater detail in the next section.

C. Oscillation frequency and linewidth

Figure 10(a) shows the measured oscillation frequency plotted against relative optical frequency detuning for two

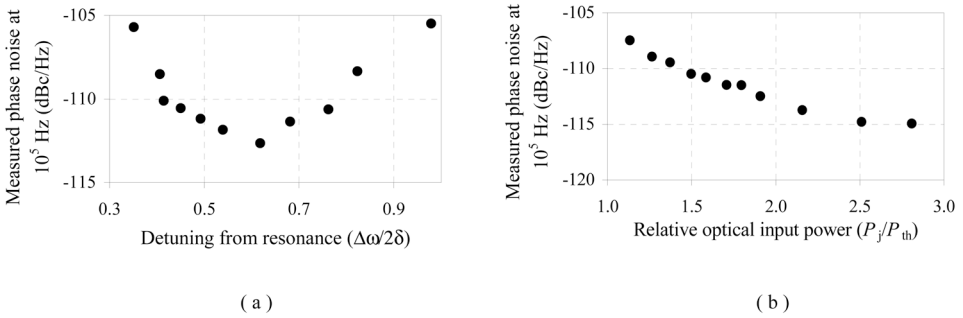

FIG. 9. (Color online) (a) Phase noise of the optomechanical oscillator measured at 10^5 Hz offset from the carrier frequency (54.2 MHz) and plotted against relative optical frequency detuning. Optical input power is about $2\times P_{\text{th}}=500$ μW. (b) Phase noise of the optomechanical oscillator measured at 10^5 Hz from the carrier frequency at $\Delta\omega/2\delta\approx 0.5$ and plotted against relative optical input power.

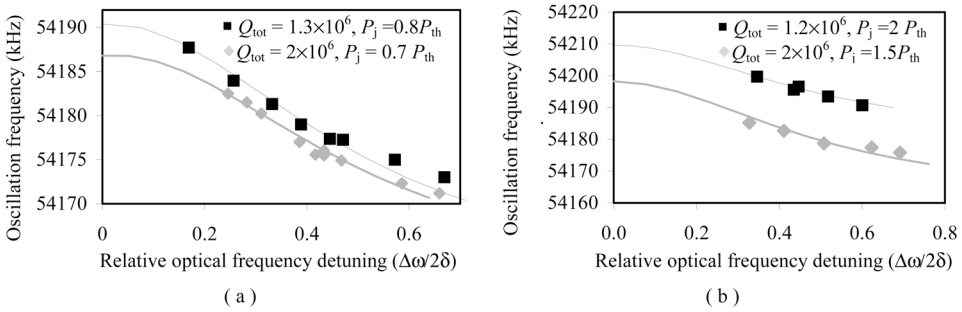

FIG. 10. (Color online) Mechanical oscillation frequency (Ω) plotted against optical frequency detuning at (a) below and (b) above threshold regimes. The solid lines are theoretical fits obtained from Eq. (7) assuming $\Omega_0 \sim 54160$ and $B/2\delta A \sim 0.05$ and 0.03 for the cases of higher and lower Q, respectively.

different optical quality factors (Q_{tot}), in the below threshold regime. The value of Q_{tot} is tuned by adjusting the gap between the fiber-taper and the microtoroid (i.e., adjusting the coupling coefficient K). Note that due to different values of Q_{tot}, the threshold optical power for self-sustained oscillations (P_{th}) is also different in each coupling regime. The solid lines are the calculated one-parameter theoretical fits obtained from substituting η_p from Eq. (7) into Eq. (4c). As explained in Appendix A the near Lorentzian behavior of oscillation frequency (Ω) versus relative optical frequency detuning ($\Delta\omega/2\delta$) indicates that the resonant frequency shift is dominated by the first term in Eq. (7) (i.e., the shift is controlled by optical absorption in the cavity). In some of our samples, we have also observed cases where the optical spring effect is dominant. Such cases will be discussed in another publication. Figure 10(b) shows the measured oscillation frequency plotted against optical frequency detuning, for two different optical quality factors, in the above threshold regime. The solid lines are the theoretical fits obtained from Eq. (7). Again the behavior of the oscillation frequency versus optical frequency detuning is governed by the thermal effect. We have used the same expressions to estimate the oscillation frequency shift both below and above threshold for the self-sustained oscillations, confirming that the mechanisms governing the variations of the resonant frequency are the same in both regimes.

The ambient temperature dependence of the oscillation frequency is another important characteristic. Indeed, in the absence of applied optical power the principal external parameter determining the oscillation frequency of each mechanical eigenmode (Ω_0) is the ambient temperature. In the linear regime ($\Delta T/T_0 \ll 1$) all thermal effects may be summarized in a single coefficient (η_T) such that

$$\Omega_0' = \Omega_0[1 + \eta_T(T - T_0)], \tag{10}$$

where Ω_0' is the natural oscillation frequency at temperature T and Ω_0 is the natural resonant frequency at temperature T_0. T and T_0 are the temperatures of the resonator that is in thermal equilibrium with the ambient atmosphere. Equation (4c) shows that at fixed values of P_j and $\Delta\omega$ the optomechanical oscillation frequency (Ω) varies only with the natural resonant frequency of the corresponding mechanical mode (Ω_0') and consequently varies with the temperature. One may estimate η_T while P_j and $\Delta\omega$ are kept constant. In our experiment we mounted the resonator structure on top of a peltier cooler so that its temperature could be controlled by adjusting the electric current supplied to the peltier. The actual temperature of the resonator structure is estimated by measuring the thermo-optical shift in the optical resonance (ω_0) [21]. At each temperature oscillation frequency was measured while the optical input power and optical frequency detuning were kept constant (The pump laser wavelength was carefully adjusted to compensate for thermo-optical shift in ω_0.) Figure 11 shows the measured oscillation frequency plotted against temperature.

The measurement is performed in the above threshold regime. The estimated value of η_T is about 6.5 kHz/K (the solid line in Fig. 11). Note that unlike the frequency shift generated by optical absorption, this thermal frequency shift is independent of the circulating optical power. Also in this case the whole structure (silicon microtoroid and the pillar) is kept at temperature T, while the case of optical absorption in the optical mode volume introduces a temperature gradient in the resonator structure.

As explained in Sec. I, unlike the oscillation frequency, the oscillation linewidth is governed by different mechanisms in the below and above threshold regimes. In order to identify these mechanisms, we have explored the behavior of the oscillation linewidth in both regimes. Figure 12 shows the measured mechanical oscillation linewidth versus optical frequency detuning at two different optical input powers and optical quality factors in the below threshold regime (in both cases $P_j \sim 0.8P_{th}$). The solid lines are the theoretical fits obtained from Eq. (4b).

The good agreement between measured and calculated results is a validation of our assumptions for linewidth derivation in this regime, namely the domination of mechanical dissipation as the line broadening mechanism. These results

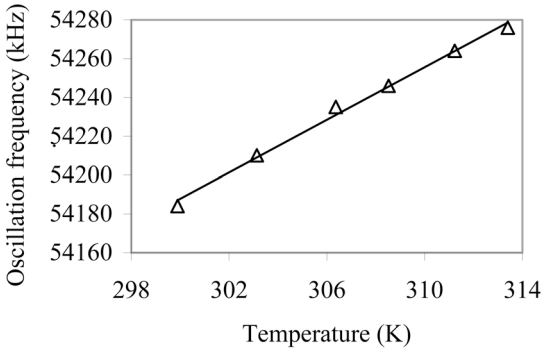

FIG. 11. (Color online) Measured oscillation frequency (Ω) plotted against the resonator temperature.

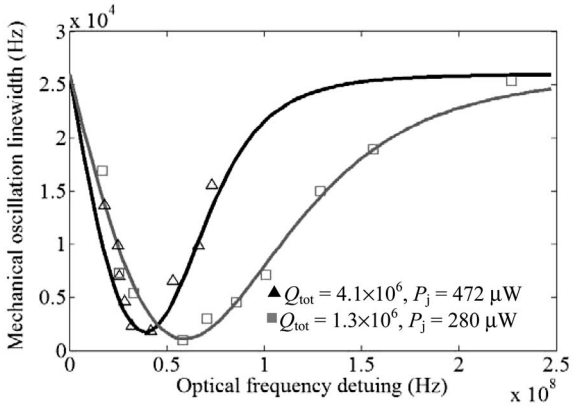

FIG. 12. Measured subthreshold mechanical oscillation linewidth as a function of optical frequency detuning from resonance. The solid lines are the theoretical fits obtained from Eq. (4b).

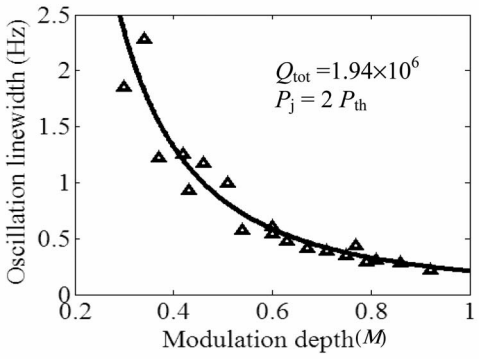

FIG. 14. Measured oscillation linewidth plotted versus modulation depth (M). The solid line is the calculated linewidth using Eq. (9).

also revalidate Eq. (5), which was previously confirmed through direct measurement of P_{th} [3].

Above threshold ($P > P_{\text{th}}$), the oscillation linewidth decreases dramatically and enters the sub-Hertz regime [Fig. 2(c)]. In this regime, as previously discussed, the oscillator has a long-term "flicker" component associated with the $1/f^3$ spectral components noted earlier as well as a short-term component exhibiting $1/f^2$ behavior (between 10^4 Hz and 10^5 Hz in our system). The latter component is associated with broadband noise in the system and can be of a fundamental origin (i.e., the fundamental contribution to linewidth). In the RF regime this fundamental noise would be the result of the thermodynamic equipartition theorem. Phase sensitive measurement at large offset frequencies ($\Delta f > 10^4$ Hz) eliminates the contribution of slow noise processes (mainly Flicker noise) and enables the study of the fundamental linewidth. The relationship between the phase noise spectral density in the $1/f^2$ regime $\mathcal{L}(\Delta f)$, and the oscillation linewidth ($\Delta\Omega$), is given by the following equation [24]:

$$\Delta\Omega = 4\pi^2 \Delta f^2 10^{\mathcal{L}(\Delta f)}, \tag{11}$$

where Δf is the frequency offset from the mechanical oscillation frequency (carrier frequency) and $\mathcal{L}$ has the units of decibels below the carrier per Hertz (dBc/Hz). Adopting the above approach, the short-term linewidth at different optical frequency detunings and optical input powers is extracted from the measured phase noise. Figure 13(a) shows the measured oscillation linewidth versus relative optical frequency detuning at $P_j = 1.5 P_{\text{th}}$. Figure 13(b) shows the measured oscillation linewidth versus relative optical input power at $\Delta\omega \approx \delta$.

These results clearly show that oscillation linewidth varies inversely with the optomechanical oscillation amplitude and consequently mechanical energy stored in the oscillator. Although this is in agreement with the general theory of line narrowing in a self-sustained oscillator, it does not yet reveal the fundamental limit for oscillation linewidth. As discussed in Sec. I, the oscillation linewidth in a thermally limited self-sustained oscillator is governed by Eq. (8). In an optomechanical oscillator this equation manifests itself as an inverse quadratic relation between optical modulation depth and the oscillation linewidth through Eq. (9). So validation of this equation is a necessary and sufficient condition for identifying the thermal noise as the fundamental limit for the oscillation linewidth. Figure 14 shows the measured oscillation linewidth versus optical modulation depth (M). This was accomplished by finely adjusting the laser pump frequency in the proximity of the optical resonance, and thereby altering the amplitude of the mechanical oscillations as well as the optical modulation depth.

The solid line is the theoretical prediction obtained from Eq. (9) ($m_{\text{eff}} \sim 2.3 \times 10^{-11}$ kg, $\Delta\omega \approx \delta$, $\Gamma_\Omega \sim 0.55$, $Q_{\text{mech}} = 2090$, and ambient temperature). The good agreement between theoretical prediction and the experimental result proves that the fundamental limit for the linewidth of a microtoroid optomechanical oscillator is actually the thermal noise in the structure.

For further confirmation of our conclusion we have mounted the microtoroid on a peltier and repeated the

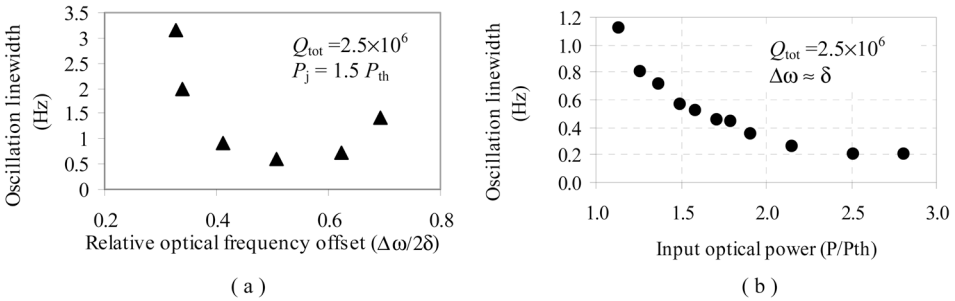

FIG. 13. (Color online) (a) Oscillation linewidth versus relative optical frequency detuning. (b) Oscillation linewidth versus relative optical input power.

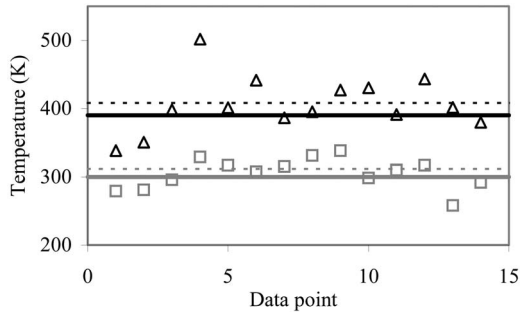

FIG. 15. Measured (solid lines) and extracted (data points) temperature for 14 data points. The actual temperatures (300 K and 390 K) are measured using a thermocouple. The extracted temperatures are calculated using the measured modulation depth (M) and oscillation linewidth ($\Delta\Omega$) in Eq. (9). The dashed lines are the average of the extracted temperatures.

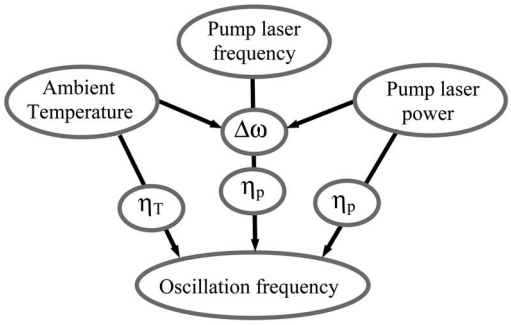

FIG. 16. Schematic diagram showing the hierarchy of the parameters that control the optomechanical oscillation frequency.

experiment above room temperature. Heating the microtoroids results in a relatively unstable behavior due to temperature fluctuation of the heating element and the convection process. Due to the difficulty of accurate measurements we were only able to measure the linewidth and oscillation amplitude at room temperature (300 K) and 90° above room temperature (390 K). At 90° above room temperature the inverse quadratic behavior of the oscillation linewidth against oscillation amplitude did not change but the oscillation linewidth was increased by an average amount of 0.2 Hz. We took 14 data points at each temperature (each data point consists of a linewidth and an amplitude) and using Eq. (9) we have extracted the effective temperatures at each data-point. Figure 15 shows the extracted temperature for each data point, the average extracted temperatures from the first and the second measurement (dotted lines) and the actual measured temperature (solid lines). This good agreement between the extracted and the measured temperatures is another indication of thermally limited oscillation linewidth.

V. PROSPECTS OF USING THE OPTOMECHANICAL OSCILLATOR AS A PHOTONIC FREQUENCY REFERENCE

A photonic frequency reference or *photonic clock* is a device that can generate a stable harmonically modulated optical field. Although one may use a standard electronic clock to modulate a laser source and generate the optical clock signal, here we use the term *photonic clock* exclusively when the optical field is directly involved in the feedback mechanism that sustains the oscillatory motion. A well-known example of such a device is an optoelectronic oscillator [26]. The optoelectronic oscillator functions based on electro-optic interaction where the feedback loop consists of an intensity modulator, optical fiber delay line, a photodetector, an amplifier, and a filter. This device can generate stable optical amplitude modulation at microwave frequencies (above 50 GHz) where most conventional electronic methods fail. However, the necessity of employing bulky and power hungry electronic and photonic devices is a serious obstacle towards monolithic fabrication of this device and using it in applications where low power consumption is critical (space missions). Radiation-pressure-driven optomechanical oscillator is essentially a radio-frequency (10–200 MHz) photonic clock that has the potential to be integrated with photonic circuits and devices. The intrinsic feedback mechanism of an optomechanical oscillator results in an exceptional simplicity, size reduction and power efficiency that is hard to achieve not only with optoelectronic oscillators but also with conventional electronic devices.

Phase noise and frequency stability are the main figures of merit in a frequency reference device. Frequency variations relative to time are indicative of oscillator stability that is usually expressed as the fractional frequency change over a time period. In an optomechanical oscillator the frequency variations are caused by changes in the ambient temperature, pump laser power (P_{in}), and pump laser frequency (ω). The ambient temperature affects the oscillation frequency by changing the natural mechanical resonant frequency (Ω_0') as well as the optical frequency detuning ($\Delta\omega$). The pump laser power and frequency affect the oscillation frequency through the optical spring effect, optical absorption and changing $\Delta\omega$. The fast variations of laser power and frequency [relative intensity noise (RIN) and frequency jitter] as well as the Brownian motion of the structure manifest themselves in the phase noise of the optomechanical oscillations while their slow variations result in optomechanical oscillation frequency drift. Figure 16 summarizes the relation among these parameters.

Usually the slow variations of laser power and frequency are stabilized by an internal feedback circuitry inside the laser. Furthermore, it has been shown that the slow variations of the optical frequency detuning ($\Delta\omega$) can be stabilized using an external feedback circuit that controls the laser wavelength to compensate for the optical resonant frequency drift [27]. Using Eqs. (4c) and (10) the fractional frequency change due variations in optical pump power, optical frequency detuning, and temperature variations can be expressed as

$$\frac{\delta\Omega}{\Omega_0} = \eta_p(\Delta\omega)\,\delta P_j, \tag{12}$$

$$\frac{\delta\Omega}{\Omega_0} = P_j \frac{d\eta_p}{d(\Delta\omega)}\,\delta(\Delta\omega), \tag{13}$$

TABLE II. Characteristics of a quartz oscillator (RALTRON) [29].

	RTXO	TCXO	OCXO
Temp. Stab (K^{-1})	$<3\times10^{-7}$	$<2\times10^{-8}$	$<3\times10^{-10}$
Power (W)	$\sim10^{-4}$[a]	$\sim5\times10^{3}$	~1

[a]Drive level.

$$\frac{\delta\Omega}{\Omega_0} = \eta_T \delta T. \tag{14}$$

As we mentioned before, $\eta_p(\Delta\omega)$ and η_T are determined by the geometry of the resonator and hence can be tailored by a careful design. For the optomechanical oscillator presented in this work $\eta_T \sim 1.3\times10^{-4}$ K^{-1}, $\eta_p(\delta)\sim 1.5\times10^{-6}$ μW^{-1}, and $d\eta_p/d(\Delta\omega)\sim 4.8\times10^{-3}$ μW^{-1} pm^{-1} (Ω_0=54200 kHz).

The closest counterpart of an optomechanical oscillator is an electromechanical oscillator that converts the dc electrical power to harmonic oscillations using a piezoelectric crystal. Although there are numerous piezoelectric crystalline substances that can serve as frequency reference, quartz, due to its desirable characteristics, has become the most widely accepted choice. Extensive research and development on quartz oscillators has dramatically improved their frequency stability and overall performance over the past 80 years. Similar to an optomechanical oscillator, one of the main causes of oscillation frequency change in a quartz oscillator is its temperature dependence [28]. The frequency change of room temperature crystal oscillators (RTXO) is minimized through the use of crystals that have been manufactured for minimum frequency change over a change in temperature. This is accomplished primarily through the choice of the crystal cut and finishing process and placing the crystal in a hermetically sealed package. The temperature compensated crystal oscillator (TCXO) uses components external to the crystal to offset the temperature effects. This could be in the form of relatively simple passive component, having opposite temperature coefficients or a combination of passive and active components that control the frequency (the crystal, the temperature compensating components, and the oscillator circuit are all encased in a hermetically sealed container). The oven controlled (OCXO) adds a heater control to the oscillator and puts the temperature-influenced elements in a hermetically insulated container. Table II shows the typical specification of three commercial quartz oscillators [29].

Following similar methods it is conceivable that one could reduce the sensitivity of the optomechanical oscillation frequency to slow temperature variations. Furthermore, the competition between two effects in the microtoroid may provide an intrinsic frequency stabilizing mechanism. Figures 10(b) and 11 show that the oscillation frequency is inversely proportional to optical frequency offset ($\Delta\omega$) and directly proportional to the ambient temperature. Since at a fixed pump laser wavelength increasing the ambient temperature increases ($\Delta\omega$), with a careful design these two mechanisms can balance each other and minimize the oscillation frequency shift.

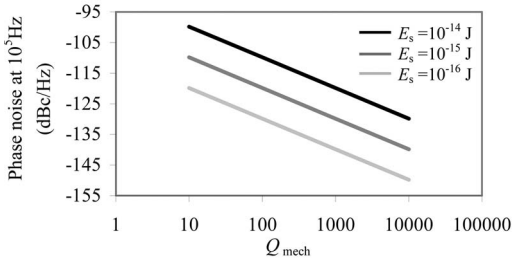

FIG. 17. Phase noise of the optomechanical oscillation plotted against mechanical Q at different oscillator energy values.

The fast variations in laser power and frequency cannot be compensated by external control and manifest themselves as high frequency ($\Delta f > 1000$ Hz) phase noise or oscillation linewidth broadening. However, as shown in Sec. III C, in an optomechanical oscillator driven by a typical semiconductor laser (RIN < -140 dB/Hz), these effects are masked by the presence of thermal noise in the microtoroid structure (Brownian motion). In our device at $P=2.5P_{\text{th}}$ and $\Delta f=10^5$ Hz the thermally limited oscillation phase noise is about -115 dBc (the best measured phase noise at this offset is -120 dBc, obtained with another microtoroid). Equation (8) shows that in this regime the oscillation linewidth and phase noise can be improved by increasing the oscillation energy and mechanical quality factor. Using Eq. (8), $\Delta\Omega$ can be restated in terms of Q_{mech}

$$\Delta\Omega = \frac{2\pi^2 kT\Omega}{E_s}\left(\frac{1}{Q_{mech}}\right), \tag{15}$$

where E_s is the total mechanical energy stored in the resonator. At each frequency offset from the carrier (Δf) this linewidth can be translated to a phase noise [Eq. (11)]. Figure 17 shows the oscillation phase noise plotted against Q_{mech} at $\Delta f=10^5$ Hz. Each order of magnitude improvement in E_s or Q_{mech} decreases the high-frequency phase noise by one order of magnitude. Usually Q_{mech} for our samples is below 5000 while the typical quality factor of a quartz oscillator is between 10^4 and 10^6.

Table III shows the phase noise of a commercial TCXO and an optomechanical oscillator (OMO) at different frequency offsets. At $\Delta f > 10^3$ Hz, the low quality factor of OMO is responsible for its relatively poor phase noise. At low frequency offsets however the extra noise in OMO noise

TABLE III. Phase noise of a typical TCXO and the OMO presented in this work at selected offset frequencies from carrier frequency ($\sim$50 MHz).

	Phase noise (dBc/Hz)	
Δf	TCXO	OMO
10^2	−110	−30
10^3	−130	−60
10^4	−140	−90
10^5	−145	−110

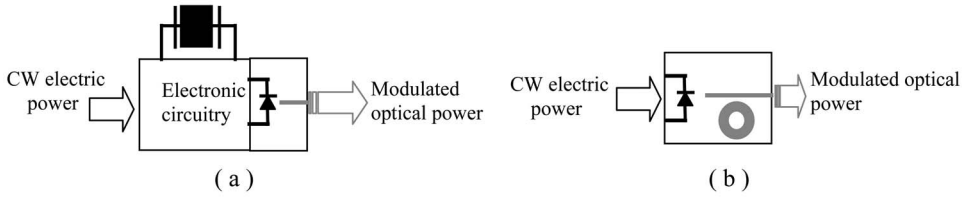

FIG. 18. (a) Optical frequency reference based on quartz oscillator. (b) Optomechanical oscillator (OMO) as a photonic clock.

is mainly environmental and due to absence of proper thermal and mechanical isolation. The mechanical quality factor of a silica microtoroid is limited by three major factors: presence of the air, bulk and surface loss mechanisms in the silica and mechanical loss through the silicon pillar. Encasing the microtoroid in a low pressure (or filled with He) hermetically sealed package can improve Q_{mech} by decreasing the external friction. The internal friction, however, is an inherent quality and can be only altered by finding a replacement material for the thermally grown silica. Note that the perfect crystal structure of the quartz results in a lower level of internal friction compared to the amorphous structure of the thermally grown silica [30]. It is well known that the physical condition of the surface can affect the quality factor of a mechanical resonator with high surface-to-volume ratio [31]. Although the surface loss in silica has not been fully explained by any single mechanism, it has been shown that the mechanical quality factor of the resonator can be improved by reducing the roughness and the overall quality of the surface [32].

The mechanical loss to the silicon pillar can be reduced by reducing the diameter of the pillar and improving the XeF_2 dry etching process to make more symmetric pillars (any deviation from circular symmetry will result in coupling among mechanical modes and hence decreases the quality factor of each mode). The mechanical energy stored in the oscillator (E_s) can be increased by increasing the laser pump power and therefore it is accompanied by a power penalty. However, at a given optical pump power the optomechanical gain ($\propto P/P_{\mathrm{th}}$) and therefore the oscillation energy increases proportional to $1/Q_{\mathrm{tot}}{}^3 Q_{\mathrm{mech}}$. So increasing the optical quality factor can dramatically improve the power efficiency for achieving a certain phase noise performance. It is important to notice that the modulation bandwidth of an optical cavity is limited by the optical quality factor [19] and therefore the maximum optomechanical frequency is always less than the resonant optical linewidth ($\Omega < \delta$ or $\Omega < \lambda_0/2Q_{\mathrm{tot}}$). This results in a trade off between high oscillation frequency and low power consumption. Theoretically, using a microtoroid resonator with $Q_0 \sim 10^8$ and $Q_{\mathrm{mech}} \sim 2000$, a 1 MHz optomechanical oscillator with a P_{th} of about 50^3 times smaller than the oscillator presented in this work (i.e., $250/50^3 \approx 2$ nW) is feasible. This suggests that the optomechanical resonator is a potential candidate for building low-power optically driven frequency references.

Figure 18 shows the schematic diagram of a quartz-based and a microtoroid-based optical clock. Due to the intrinsic feedback mechanism and all-optical operation, using the optomechanical oscillator reduces the complexity of the system by eliminating the electronic feedback circuitry.

Also the small size (micron size) and on-chip nature of the optomechanical oscillator makes it a perfect candidate for integration with photonic devices while quartz oscillators are usually encased in millimeter-size surface mount packages and cannot be integrated with the driving circuit. Moreover, for certain applications the high-efficiency of the diode lasers combined with the low threshold power for optomechanical oscillations may result in power efficiencies comparable with low power electronic clocks.

Another advantage of the optomechanical oscillator is its immunity against external electromagnetic radiation. The optical nature of the microtoroid mechanical oscillator combined with the fact that it is made of nonpiezoelectric material makes it noticeably less susceptible to electromagnetic perturbations compared to a quartz oscillator.

It is worth noting that throughout this paper we have assumed that the optical coupling coefficient is constant and noiseless. However, the fiber taper with a diameter of less than 1 micron is also a micromechanical oscillator that is actuated both thermally and through noises in the nanopositioner. This can cause fluctuations in the optical coupling factor and manifest itself as optomechanical frequency fluctuations through variations in the circulating optical power. So even at room temperature and without employing any external control mechanism, replacing the taper coupling with a robust coupling mechanism may dramatically improve the stability of the optomechanical oscillator.

VI. CONCLUSION

We have studied the effect of the optical frequency detuning ($\Delta\omega$), optical input power (P_j) and temperature on the frequency spectrum, phase noise, oscillation linewidth, and oscillation frequency of a microtoroidal optomechanical oscillator. Through these studies we have identified the principal mechanisms through which $\Delta\omega$ and P_j control the oscillation characteristics below and above the threshold for self-sustained oscillations. In both regimes we have derived closed form expressions for oscillation frequency and linewidth that can significantly simplify the comparison between experimental data and theoretical predictions. With minor modification and proper interpretation of the physical parameters our approach can be adopted in other optomechanical oscillators and provides the foundation for improving their performance.

The outcome of our measurements shows that for a typical microtoroid resonator, *assuming* that optical pump power is $1.5P_{\mathrm{th}}$ with an optical detuning equal to half the bandwidth of the optical resonance (δ) optomechanical oscillation has a relatively clean spectrum (>10 dB second harmonic suppression ratio) with an oscillation linewidth in subhertz regime.

It has been shown that the oscillation frequency is governed by the ambient temperature as well as the circulating

power in the optical cavity. Using the semiempirical expressions one can estimate the frequency sensitivity of the optomechanical oscillator to the pump laser power and wavelength as well as fluctuation in the ambient temperature. Our measurement results have also confirmed that the fundamental limit of the oscillation linewidth is set by the presence of Brownian noise in the optomechanical oscillator.

Preliminary estimations show that encasing the optomechanical oscillator in a hermetically sealed package and improving the optical and mechanical quality of the toroid microresonator may result in a relatively stable and reliable photonic-clock. All-optical operation, immunity to electromagnetic radiation, low-power consumption, small volume, and on-chip fabrication are among the unique properties of this new type of oscillator that may be beneficial in certain applications.

APPENDIX A: DERIVATION OF η_P

In the presence of circulating optical power the mechanical resonant frequency of a toroidal resonator is modified by two major processes: the optical spring effect and optical absorption.

1. Optical spring effect

The presence of the radiation pressure force in the microtoroid structure increases the effective spring constant of the flexural mechanical eigenmodes. The contribution of radiation pressure in the spring constant (k_{os}) is referred to as the *optical spring effect* [14]. In the adiabatic regime ($\Omega_0 \ll 2\delta$), one may calculate k_{os} using the relations among radiation force, circulating optical power and optical power at the coupling junction [25,10]:

$$k_{os} = -\frac{d}{dr}F_{rad}, \tag{A1}$$

$$F_{rad} = \frac{2\pi n}{c}P_{circ}, \tag{A2}$$

$$P_{circ} = \frac{\lambda Q_{tot}^2}{\pi^2 n R_0 Q_{\text{ext}}}\frac{\delta^2}{\Delta\omega^2 + \delta^2}P_j, \tag{A3}$$

$$k_{os} = \frac{2\omega_0^2}{R_0^2 Q_{\text{ext}}}\frac{\Delta\omega}{(\Delta\omega^2 + \delta^2)^2}P_j. \tag{A4}$$

Equations (A1)–(A3) imply as lead in to Eq. (4).

The oscillation frequency can be estimated as

$$\Omega = \sqrt{\frac{k_{os} + k_0}{m_{eff}}} = \sqrt{\frac{k_{os} + m_{eff}\Omega_0^2}{m_{eff}}}, \tag{A5}$$

assuming $\Omega + \Omega_0 \approx 2\Omega_0$ we have:

$$\Omega - \Omega_0 \approx \frac{k_{os}}{2\Omega_0 m_{eff}}, \tag{A6}$$

where k_0 is the spring constant in the absence of the optical power.

2. Thermal effect

The resonant frequency of a mechanical eigenmode of the microtoroid resonator assuming displacements $\Delta R \ll R_0$ can be written as

$$\Omega = G + NR, \tag{A7}$$

where R is the microtoroid radius, and G and N are determined by the geometry of the microtoroid as well as its material properties. When the circulating optical power is zero, the resonant frequency of the isolated resonator is $\Omega_0 = G + NR_0$.

When the resonator is coupled to an optical waveguide, absorption of the circulating optical power (P_{circ}) in the microtoroid creates a temperature gradient in the structure proportional to P_{circ}. The associated thermal expansion of the microtoroid radius can be expressed in terms of an effective temperature increment: $\Delta R_T = R_0 \beta \Delta T$ (where β is the linear expansion coefficient of silica). When $\Delta R_T \ll R_0$

$$\Omega = \Omega_0 + \beta \Delta T N R_0. \tag{A8}$$

ΔT is the temperature increment due to optical absorption in the microtoroid, which is proportional to the circulating optical power (P_{circ})

$$\Delta T = \Lambda P_{\text{cric}}, \tag{A9}$$

where Λ is the proportionality factor between the circulating optical power and the temperature increment. Using Eqs. (A3), (A8), and (A9) the frequency shift due to optical absorption can be written as

$$\Omega - \Omega_0 = N R_0 \beta \Lambda \frac{\lambda Q_{\text{tot}}^2}{\pi^2 n R_0 Q_c}\frac{\delta^2}{\Delta\omega^2 + \delta^2}P_j. \tag{A10}$$

Now we can combine Eqs. (A4), (A6), and (A10) to derive η_p such that

$$\Omega = \Omega_0[1 + \eta_P(\Delta\omega)P_j]. \tag{A11}$$

Since we are mainly interested in the $\Delta\omega$ dependence of η_p it is useful to write it in the following form:

$$\eta_P = A\left(\frac{1}{\Delta\omega^2 + \delta^2}\right) + B\left[\frac{\Delta\omega}{(\Delta\omega^2 + \delta^2)^2}\right], \tag{A12}$$

$$A = \frac{\lambda\beta N \Lambda \delta^2 Q_{\text{tot}}^2}{\pi^2 n Q_{\text{ext}}}, \tag{A13}$$

$$B = \frac{\omega_0^2}{\Omega_0 m_{\text{eff}} R_0^2 Q_{\text{ext}}}. \tag{A14}$$

Equation (A12) can be rewritten in terms of relative optical frequency detuning ($d = \Delta\omega/2\delta$)

$$\eta_P = \frac{1}{4\delta^2}\left[\left(\frac{1}{d^2 + 1/4}\right) + \frac{B}{2\delta A}\left(\frac{d}{(d^2 + 1/4)^2}\right)\right]. \tag{A15}$$

Figure 19 shows η_p plotted against d for three different values of $B/2\delta A$ (η_p is normalized to its maximum value for each curve). When $B/2\delta A > 5$ the behavior of η_p is dominated by the second term in Eq. (A15) (i.e., optical spring

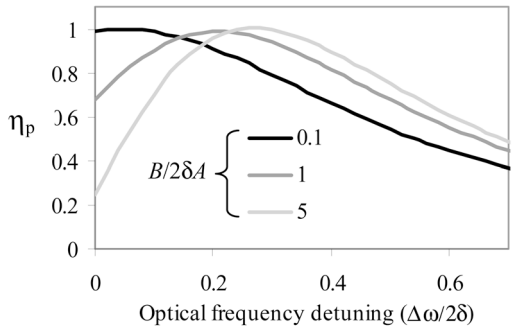

FIG. 19. (Color online) η_p plotted against $d=\Delta\omega/2\delta$ for three different values of $B/2\delta A$.

effect dominates. Note that k_{os} has a maximum at $d=0.3$). When $B/2\delta A<0.1$, the behavior of η_p is dominated by the first term in Eq. (A15) (thermal effect) and the mechanical resonant frequency is essentially proportional to the circulating optical power in the cavity (P_{circ}).

It is worth mentioning that in a damped harmonic oscillator the resonant frequency is also affected by the magnitude of loss in the resonator

$$\Omega=\Omega_0\sqrt{1-\frac{\gamma^2}{4\Omega_0^2}}. \tag{A16}$$

Since γ is a function of detuning and optical input power [Eq. (4b)] so below threshold Eq. (A16) introduces another mechanism through which the oscillation frequency is affected by P_j and $\Delta\omega$. But experimental results and theoretical calculations show that $\gamma/2\Omega_0$ is usually in the order of 10^{-4} and the frequency shift $(\Omega-\Omega_0)$ is in the order of 10^{-2} kHz that is negligible compared to frequency shifts that we observe in the experiment.

APPENDIX B: RELATION BETWEEN OSCILLATION AMPLITUDE AND MODULATION DEPTH

The linewidth for a thermally limited oscillator is given as

$$\Delta\Omega=\frac{k_BT}{2P_d}(\Delta\Omega_0)^2, \tag{B1}$$

where P_d is the oscillator output power (or power delivered to the resistive load in the case of an electrical oscillator). In a mechanical oscillator, P_d is the dissipated power

$$P_d=\frac{E_{\text{stored}}\Omega_0}{Q_{\text{mech}}}=(1/2)m_{\text{eff}}\Omega^2r_{\text{max}}^2\Delta\Omega_0. \tag{B2}$$

Substituting (B2) into (B1)

$$\Delta\Omega=\frac{k_BT}{m_{\text{eff}}\Omega_0^2r^2}\Delta\Omega_0. \tag{B3}$$

The radial displacement (ΔR) and the modulated optical power (P_{mod}) are related through the following equation:

$$\Gamma(\Omega_0)\Delta R\approx\left(\frac{R_0}{\omega_0}\right)\left(\frac{P_{\text{mod}}}{S(\Delta\omega)}\right), \tag{B4}$$

where $\Gamma(\Omega_0)$ is the optical modulation transfer function [19] and $S(\Delta\omega)$ is the slope of the optical power transmission function at $\Delta\omega$.

For a high-Q optical mode and $\Delta\omega\sim\delta$, $S(\Delta\omega)\sim P_{\text{max}}/2\delta$ so (B4) can be restated in terms of the optical modulation depth M (see Fig. 20):

$$\Delta R\approx\left(\frac{R_0}{Q_{\text{tot}}}\right)\left(\frac{M}{\Gamma(\Omega_0)}\right)=\frac{MR_0}{\Gamma(\Omega_0)Q_{\text{tot}}}, \tag{B5}$$

where $M=P_{\text{mod}}/P_{\text{max}}$. Knowing ΔR is equal to $2r_{\text{max}}$ (where r_{max} is the amplitude of the mechanical displacement in the radial direction), $\Delta\Omega$ can be expressed in terms of the modulation depth (M) by substituting Eq. (B5) into (B3)

$$\Delta\Omega=\left(\frac{4k_BTQ_{\text{tot}}^2}{m_{\text{eff}}\Omega_0^2R_0^2}\right)\frac{\Gamma^2(\Omega_0)\Delta\Omega_0}{M^2}. \tag{B6}$$

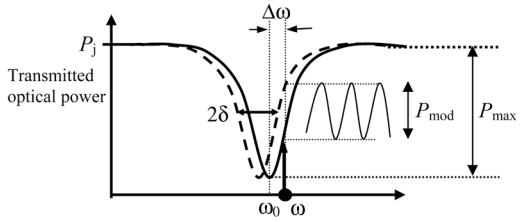

FIG. 20. (Color online) Schematic diagram showing the relation between modulation depth and optical frequency shift.

[1] H. Rokhsari, T. J. Kippenberg, T. Carmon, and K. J. Vahala, Opt. Express **13**, 14 (2005).
[2] T. Carmon, H. Rokhsari, L. Yang, T. J. Kippenberg, and K. J. Vahala, Phys. Rev. Lett. **94**, 223902 (2005).
[3] T. J. Kippenberg, H. Rokhsari, T. Carmon, A. Scherer, and K. J. Vahala, Phys. Rev. Lett. **95**, 033901 (2005).
[4] A. Cho, Science **309**, 366 (2005).
[5] D. K. Armani, T. J. Kippenberg, S. M. Spillane, and K. J. Vahala, Nature (London) **421**, 925 (2003).
[6] I. Tittonen *et al.*, Phys. Rev. A **59**, 1038 (1999).
[7] R. Fermani, S. Mancini, and P. Tombesi, Phys. Rev. A **70**, 045801 (2004).
[8] S. Mancini, V. Giovannetti, D. Vitali, and P. Tombesi, Phys. Rev. Lett. **88**, 120401 (2002).
[9] D. Rugar and P. Grutter, Phys. Rev. Lett. **67**, 699 (1991).
[10] S. M. Spillane, PhD thesis, Caltech, 2004.
[11] S. M. Spillane, T. J. Kippenberg, O. J. Painter, and K. J. Vahala, Phys. Rev. Lett. **91**, 043902 (2003).

[12] X. Liu, J. F. Vignola, D. M. Photiadis, A. Sarkissian, B. H. Houston, R. D. Merithew, and R. O. Pohl, Physica B **316**, 393 (2002).
[13] F. R. Blom, S. Bouwstra, M. Elwenspoek, and J. H. J. Fluitman, J. Vac. Sci. Technol. B **10**, 19 (1992).
[14] S. W. Schediwy, C. Zhao, L. Ju *et al.*, Class. Quantum Grav. **21**, 1253 (2004).
[15] A. L. Schawlow and C. H. Townes, Phys. Rev. **112**, 1940 (1958).
[16] W. A. Edson, Proc. Radio Engineers **48**, 1454 (1960).
[17] F. Herzel, IEEE Circuits Syst. Mag. **45**, 904 (1998).
[18] H. Rokhsari, M. Hossein-Zadeh, and K. J. Vahala, "Brownian motion in Radiation-Pressure-Driven Micromechanical Oscillators," Frontiers in Optics Conference 2005, PDP-B, FiO Post deadline Papers II.
[19] When the optical path length in an optical resonator is modulated, the finite response time of the resonator is translated to a low-pass filter function. We call this filter function "optical modulation transfer function" of the resonator or $\Gamma_\Omega=\Gamma(\Omega)$. $\Gamma(\Omega)$ can be estimated by solving the dynamical equation for the circulating optical field inside a resonator while the path length is modulated at frequency Ω.
[20] M. Cai, O. Painter, and K. J. Vahala, Phys. Rev. Lett. **85**, 74 (2000).
[21] T. Carmon, L. Yang, and K. J. Vahala, Opt. Express **12**, 4742 (2004).
[22] A. Hajimiri and T. H. Lee, IEEE J. Solid-State Circuits **33**, 179 (1998).
[23] D. B. Leeson, Proc. IEEE **54**, 329 (1966).
[24] *The Design of Low Noise Oscillators*, edited by A. Hajimiri and T. H. Lee (Kluwer, Dordrecht, 1999).
[25] H. Rokhsari, T. J. Kippenberg, T. Carmon, and K. J. Vahala, IEEE J. Sel. Top. Quantum Electron. **12**, 96 (2006).
[26] X. S. Yao and L. Maleki, J. Opt. Soc. Am. B **13**, 1725 (1996).
[27] T. Carmon, T. J. Kippenberg, L. Yang, H. Rokhsari, S. M. Spillane, and K. J. Vahala, Opt. Express **13**, 3558 (2005).
[28] "Fundamentals of Quartz Oscillators," Application Note 200-2, Hewlett Packard.
[29] RALTRON oscillators, series AS-SMD, OCXO 8000, RTX-206 (www.raltron.com).
[30] A. Seed, Br. J. Appl. Phys. **16**, 87 (1965).
[31] Steven D. Penn, Alexander Agreev, Dan Busby, Gregory M. Harry, Andri M. Gretarsson, Kenji Numata, and Phil Willems, Phys. Lett. A **A352**, 3 (2006).
[32] Alexander Ageev, Belkis Cabrera Palmer, Antonio De Felice, Steven D. Penn, and Peter R. Saulson, Class. Quantum Grav. **21**, 3887 (2004).